Abstracta

Ano XVIII - N. 01

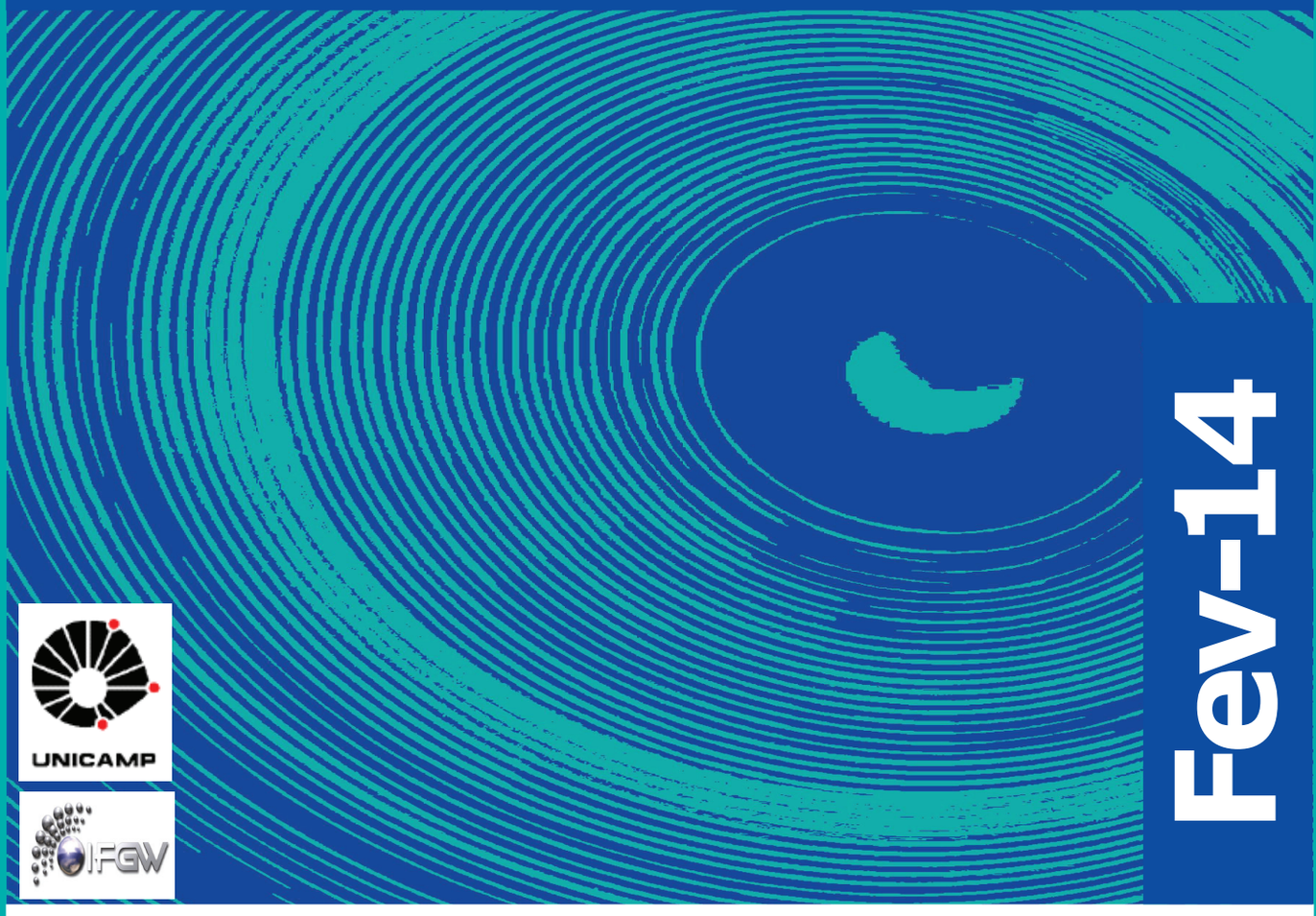

Fev-14

UNICAMP

IFGW

Trabalhos Publicados

[P001-2014] "A comparison between Geant4 PIXE simulations and experimental data for standard reference samples"

Francis, Z.; El Bast, M.; El Haddad, R.; Mantero, A.; Incerti, S.; Ivanchenko, V.; El Bitar, Z.; Champion, C.; **Bernal, M. A.***; Roumie, M.

The Geant4 PIXE de-excitation processes are used to simulate proton beam interactions with sample materials of known composition. Simulations involve four mono-elemental materials; Cu, Fe, Si and Al and three relatively complex materials: stainless steel, phosphor bronze and basal BE-N reference material composed of 25 different elements. The simulation results are compared to experimental spectra acquired for real samples analyzed using 3 MeV incident protons delivered by an ion tandem accelerator. Data acquisition was performed using a Si(Li) detector and an aluminum funny filter was added for the three last mentioned samples depending on the configuration to reduce the noise and obtain clear resulting spectrum. The results show a good agreement between simulations and measurements for the different samples.

Nuclear Instruments & Methods In Physics Research Section B-Beam Interactions With Materials And Atoms 316[1-5], 2013. DOI:10.1016/j.nimb.2013.08.006

[P002-2014] "A method for choosing the smoothing parameter in a semi-parametric model for detecting change-points in blood flow"

Han, S. W.; **Mesquita, R. C.***; Busch, T. M.; Putt, M. E.

In a smoothing spline model with unknown change-points, the choice of the smoothing parameter strongly influences the estimation of the change-point locations and the function at the change-points. In a tumor biology example, where change--points in blood flow in response to treatment were of interest, choosing the smoothing parameter based on minimizing generalized cross-validation (GCV) gave unsatisfactory estimates of the change-points. We propose a new method, aGCV, that re-weights the residual sum of squares and generalized degrees of freedom terms from GCV. The weight is chosen to maximize the decrease in the generalized degrees of freedom as a function of the weight value, while simultaneously minimizing aGCV as a function of the smoothing parameter and the change-points. Compared with GCV, simulation studies suggest that the aGCV method yields improved estimates of the change-point and the value of the function at the change-point.

Journal Of Applied Statistics 41[1], 26-45, 2014. DOI: 10.1080/02664763.2013.830085

[P003-2014] "A study on analytic parametrizations for proton-proton cross-sections and asymptotia"

Menon, M. J.*; Silva, P. V. R. G.*

A comparative study on some representative parametrizations for the total and elastic cross-sections as a function of energy is presented. The dataset comprises pp and (p) over barp scattering in the c.m. energy interval 5 GeV-8 TeV. The parametrization for the total cross-section at low and intermediate energies follows the usual reggeonic structure (non-degenerate trajectories). For the leading high-energy pomeron contribution, we consider three distinct analytic parametrizations: either a power (P) law, or a log-squared (L2) law or a log-raised- to-gamma (L gamma) law, where the exponent gamma is treated as a real free fit parameter. The parametrizations are also extended to fit the elastic (integrated) cross-section data in the same energy interval. Our main conclusions are the following: (1) the data reductions with the logarithmic laws show strong dependence on the unknown energy scale involved, which is treated here either as a free parameter or fixed at the energy threshold; (2) the fit results with the P law, the L2 law (free scale) and the L gamma law (fixed scale and exponent gamma above 2) are all consistent within their uncertainties and with the experimental data up to 7 TeV, but they partially underestimate the high-precision TOTEM measurement at 8 TeV; (3) once compared with these results, the L2 law with fixed scale is less consistent with the data and, in the case of a free scale, this pomeron contribution decreases as the energy increases below the scale factor (which lies above the energy cutoff); (4) in all cases investigated, the predictions for the asymptotic ratio between the elastic and total cross-sections, within the uncertainties, do not exceed the value 0.430 (therefore, below the black--disc limit) and the results favor rational limits between 1/3 and 2/5. We are led to conclude that the rise of the hadronic cross-sections at the highest energies still constitutes an open problem, demanding further and detailed investigation.

Journal Of Physics G-Nuclear And Particle Physics 40[12], 125001, 2013. DOI: 10.1088/0954-3899/40/12/125001

[P004-2014] "An atomistic geometrical model of the B-DNA configuration for DNA-radiation interaction simulations"

Bernal, M. A.*; Sikansi, D.*; Cavalcante, F.*; Incerti, S.; Champion, C.; Ivanchenko, V.; Francis, Z.

In this paper, an atomistic geometrical model for the B-DNA configuration is explained. This model accounts for five organization levels of the DNA, up to the 30 nm chromatin fiber. However, fragments of this fiber can be used to construct the whole genome. The algorithm developed in this work is capable to determine which is the closest atom with respect to an arbitrary point in space. It can be used in any application in which a DNA geometrical model is needed, for instance, in investigations related to the effects of ionizing radiations on the human genetic material. Successful consistency checks were carried out to test the proposed model. Program summary Program title: FindClosestAtom Catalogue identifier: AEPZ_v1_0 Program summary URL: http://cpc.cs.qub.ac.uk/summaries/AEPZ_v1_0.html. Program obtainable from: CPC Program Library, Queen's University, Belfast, N. Ireland Licensing provisions: Standard CPC licence, http://cpc.cs.qub.ac.uk/licence/licence.html
No. of lines in distributed program, including test data, etc.: 1245 No. of bytes in distributed program, including test data, etc.: 6574 Distribution format: tar.gz Programming language: FORTRAN. Computer: Any. Operating system: Multi-platform.
RAM: 2 Gb Classification: 3. Nature of problem: The Monte Carlo method is used to simulate the interaction of ionizing radiation with the human genetic material in order to determine DNA damage yields per unit absorbed dose. To accomplish this task, an algorithm to determine if a given energy deposition lies within a given target is needed. This target can be an atom or any other structure of the genetic material. Solution method: This is a stand-alone subroutine describing an atomic-resolution geometrical model of the B-DNA configuration. It is able to determine the closest atom to an arbitrary point in space. This model accounts for five organization levels of the human genetic material, from the nucleotide pair up to the 30 nm chromatin fiber. This subroutine carries out a series of coordinate transformations to find which is the closest atom containing an arbitrary point in space. Atom sizes are according to the corresponding van der Waals radii. Restrictions: The geometrical model presented here does not include the chromosome organization level but it could be easily build up by using fragments of the 30 nm chromatin fiber. Unusual features: To our knowledge, this is the first open source atomic-resolution DNA geometrical model developed for DNA-radiation interaction Monte Carlo simulations.

In our tests, the current model took into account the explicit position of about 56 x 10(6) atoms, although the user may enhance this amount according to the necessities. Running time: This subroutine can process about 2 million points within a few minutes in a typical current computer.

Computer Physics Communications 184[12], 2840-2847, 2013. DOI: 10.1016/j.cpc.2013.07.015

[P005-2014] "Angular analysis and branching fraction measurement of the decay B-0 -> K*(0)mu(+)mu(-)"

Chatrchyan, S (Chatrchyan, S.); Khachatryan, V (Khachatryan, V.); Sirunyan, AM (Sirunyan, A. M.); Tumasyan, A (Tumasyan, A.); **Chinellato, J.*; Manganote, E. J. Tonelli***; et al.
CMS Collaboration

The angular distributions and the differential branching fraction of the decay B-0 -> K*(892)(0)mu(+)mu(-) are studied using a data sample corresponding to an integrated luminosity of 5.2 fb(-1) collected with the CMS detector at the LHC in pp collisions at root s = 7 TeV. From more than 400 signal decays, the forward-backward asymmetry of the muons, the K*(892)(0) longitudinal polarization fraction, and the differential branching fraction are determined as a function of the square of the dimuon invariant mass. The measurements are in good agreement with standard model predictions.

Physics Letters B 727[1-3], 77-100, 2013. DOI: 10.1016/j.physletb.2013.10.017

[P006-2014] "Anisotropic magnetocaloric effect in ErGa2 and HoGa2 single-crystals"

dos Reis, R. D.*; da Silva, L. M.; dos Santos, A. O.; Medina, A. M. N.; **Cardoso, L. P.*; Gandra, F. C. G.***

In this work we study the anisotropic magnetocaloric properties of ErGa2 and HoGa2 single-crystals. Both compounds present antiferromagnetic ordering below 10 K but with different easy axis as a result of the crystal field anisotropy. The single--crystal conventional MCE values are similar or in certain circumstances even larger than the results for the polycrystalline material. The anisotropic MCE was calculated by taking the difference of the entropy change of the easy and hard magnetization directions. For both compounds, the anisotropic variation of entropy is as large as the conventional entropy change obtained by sweeping the magnetic field up to 5 T. Particularly for ErGa2 an inverse MCE for a 3 T field oriented along the easy axis is obtained with similar magnitude of the 5 T MCE found for polycrystalline samples. The results show that by exploring anisotropic properties of the materials it is possible to obtain a significant MCE. From a technological point of view this can be an interesting alternative because the MCE is produced just by rotating the magnetic material under a constant magnetic field.

Journal Of Alloys And Compounds 582, 461-465, 2014. DOI: 10.1016/j.jallcom.2013.08.023

[P007-2014] "Anisotropy of the field-induced kinetic energy density in Bi2212"

Pena, J. P.; **da Silva, R. R.***; Pureur, P.

We present an experimental study of the in field kinetic energy density in two Bi2Sr2CaCu2O8 broken vertical bar delta single crystals. The kinetic energy density is determined from magnetization measurements performed above the irreversibility line. Anisotropy effects are observed when an external magnetic field is applied in the direction perpendicular or parallel to the superconducting Cu-O-2 planes. When the held is applied parallel to the c-axis, the most relevant contribution to the kinetic energy comes from the Abrikosov vortices. At low fields, an additional tel related to granularity is also observed. A kink in the kinetic energy density associated to the decoupling of the superconducting layers is identified when the held is applied parallel to the oh planes.

Physica B-Condensed Matter 433, 79-83, 2014. DOI: 10.1016/j.physb.2013.10.025

[P008-2014] "Anomalous strain behavior on EuTe self-assembled islands"

Heredia, E.*; Diaz, B.*; Malachias, A.*; Rappl, P. H. O.*; Iikawa, F.*; Brasil, M. J. S. P.***; Motisuke, P.***

EuTe is a magnetic semiconductor with potential applications in prototype optoelectronic and spintronic devices. In this work, we investigated the structural properties of EuTe grown on BaF2(111) substrates by molecular beam epitaxy. X-ray diffraction measurements were performed on two series of samples with different growth times and temperatures. The growth occurs in the Volmer-Webber mode, with initial formation of islands that then coalesce to form thin films. The islands size, mosaic spread, and strain state are deduced as a function of growth conditions. Surprisingly, the EuTe islands exhibit in-plane tensile strain, while compressive strain is expected for structures grown over a substrate with smaller lattice parameter. The islands tensile strain relaxes with increasing deposition times and substrate temperature, and it tends to zero for thick EuTe films. We propose that the EuTe/BaF2 lattice mismatch is compensated by the formation of interfacial misfit dislocations. The growth conditions out of equilibrium favor the formation of a metastable state with a high concentration of dislocations that over-compensates the original misfit. This is in agreement with the observed reduction of tensile strain as the substrate temperature increases.

Journal Of Crystal Growth 386, 139-145, 2014. DOI: 10.1016/j.jcrysgro.2013.10.002

[P009-2014] "Are IceCube neutrinos unveiling PeV-scale decaying dark matter?"

Esmaili, A.*; Serpico, P. D.

Recent observations by IceCube, notably two PeV cascades accompanied by events at energies similar to (30-400) TeV, are clearly in excess over atmospheric background fluxes and beg for an astroparticle physics explanation. Although some models of astrophysical accelerators can account for the observations within current statistics, intriguing features in the energy and possibly angular distributions of the events make worth exploring alternatives. Here, we entertain the possibility of interpreting the data with a few PeV mass scale decaying dark matter, with lifetime of the order of 10(27) s. We discuss generic signatures of this scenario, including its unique energy spectrum distortion with respect to the benchmark E-v(-2) expectation for astrophysical sources, as well as peculiar anisotropies. A direct comparison with the data show a good match with the above-mentioned features. We further discuss possible future checks of this scenario.

Journal Of Cosmology And Astroparticle Physics 11, 054, 2013. DOI: 10.1088/1475-7516/2013/11/054

[P010-2014] "Bulk plasmon polariton-gap soliton-induced transparency in one-dimensional Kerr-metamaterial superlattices"

Cavalcanti, S. B.; **Brandao, P. A.*;** Bruno-Alfonso, A.; **Oliveira, L. E.***

We have performed a theoretical study of various arrangements of one-dimensional heterostructures composed by bilayers made of nondispersive (A)/dispersive linear (B) materials and illuminated by an obliquely incident electromagnetic wave, which are shown to exhibit a robust bulk-like plasmon-polariton gap for frequencies below the plasma frequency. The origin of this gap stems from the coupling between photonic and plasmonic modes that may be of a magnetic (electric) origin in a transversal electric (traversal magnetic) configuration yielding a plasmon-polariton mode. By substituting the nondispersive linear layer by a nonlinear Kerr layer, we have found that, for frequencies close to the edge of the plasmon-polariton gap, the transmission of a finite superlattice presents a multistable behavior and it switches from very low values to the maximum transparency at particular values of the incident power. At these frequencies, for those singular points where transmission becomes maximum, we find localized plasmon-polariton-gap solitons of various orders depending on the particular value of the incident power. Present results reveal, therefore, new gap plasmon-soliton solutions that are hybrid modes stemming from the resonant coupling between the incoming electromagnetic wave and the plasmonic modes of the dispersive material, leading to the transparency of a stack with nonlinear inclusions.

Optics Letters 39[1], 178-181, 2014. DOI: 10.1364/OL.39.000178

[P011-2014] "Carrier saturation in multiple quantum well metallo-dielectric semiconductor nanolaser: Is bulk material a better choice for gain media?"

Vallini, F.*; Gu, Q.; Kats, M.; Fainman, Y.; **Frateschi, N. C.***

Although multi quantum well (MQW) structure is frequently suggested as the appropriate medium for providing optical gain in nanolasers with low threshold current, we demonstrate that in general bulk gain medium can be a better choice. We show that the high threshold gain required for nanolasers demands high threshold carrier concentrations and therefore a highly degenerate condition in which the barriers between the quantum wells are heavily pumped. As a result, there occurs spontaneous emission from the barrier in very dissipative low Q modes or undesired confined higher Q modes with resonance wavelengths close to the barrier bandgap. This results in a competition between wells and barriers that suppresses lasing. A complete model involving the optical properties of the resonant cavity combined with the carrier injection in the multilayer structure is presented to support our argument. With this theoretical model we show that while lasing is achieved in the nanolaser with bulk gain media, the nanolaser with MQW gain structure exhibits well emission saturation due to the onset of barrier emission.

Optics Express 21[22], 25985-25998, 2013. DOI: 10.1364/OE.21.025985

[P012-2014] "Centrality dependence of the pseudorapidity density distribution for charged particles in Pb-Pb collisions at root s(NN)=2.76 TeV"

Abbas, E.; Abelev, B.; Adam, J.; Adamova, D.; Adare, A. M.; **Dash, A.*; Takahashi, J.***; et al.
ALICE Collaboration

We present the first wide-range measurement of the charged-particle pseudorapidity density distribution, for different centralities (the 0-5%, 5-10%, 10-20%, and 20-30% most central events) in Pb-Pb collisions at root s(NN) = 2.76 TeV at the LHC. The measurement is performed using the full coverage of the ALICE detectors, -5.0 < eta < 5.5, and employing a special analysis technique based on collisions arising from LHC 'satellite' bunches. We present the pseudorapidity density as a function of the number of participating nucleons as well as an extrapolation to the total number of produced charged particles (N-ch = 17165 +/- 772 for the 0-5% most central collisions). From the measured dN(ch)/d eta distribution we derive the rapidity density distribution, dN(ch)/dy, under simple assumptions. The rapidity density distribution is found to be significantly wider than the predictions of the Landau model. We assess the validity of longitudinal scaling by comparing to lower energy results from RHIC. Finally the mechanisms of the underlying particle production are discussed based on a comparison with various theoretical models.

Physics Letters B 726[4-5], 610-622, 2013. DOI: 10.1016/j.physletb.2013.09.022

[P013-2014] "Characterization and Shelf Life of beta-Carotene Loaded Solid Lipid Microparticles Produced With Stearic Acid and Sunflower Oil"

Gomes, G. V. D.; Borrin, T. R.; **Cardoso, L. P.***; Souto, E.; de Pinho, S. C.

Solid lipid microparticles were tested as microencapsulation systems for protecting beta-carotene from degradation. Blends of long-chain (C18) solid lipids (70% stearic acid) and sunflower oil (30%) were used to produce lipid microparticles encapsulating the carotenoid. Polysorbate 80 (4%) was employed to stabilize the stearic acid microparticles. The concentration of beta-carotene was monitored using spectrophotometry, the particle size distribution was measured by laser diffraction, the crystal structure was determined by wide angle X-ray diffraction (WAXD), and the thermal behaviour was characterized by differential scanning calorimetry (DSC) over a period of seven months. All of the systems had an average particle size smaller than 5 mu m. To avoid beta-carotene oxidation, alpha-tocopherol was added to the formulations and its action as an oxygen trap was crucial for the antioxidant effect. For stearic-acid microparticles with alpha-tocopherol, more than 90% of the initial amount of beta-carotene was preserved after seven months under refrigerated storage (7-10 degrees C) in the dark. Significant microstructural alterations were detected using WAXD and DSC only in the stearic acid microparticles without alpha--tocopherol. These results seemed promising and suggested that the blends of long-chain solid lipids and liquid lipids were suitable for the production of stable solid lipid microparticles.

Brazilian Archives Of Biology And Technology 56[4], 663-671, DOI: 10.1590/S1516-89132013000400017

[P014-2014] "Charmonium and e(+)e(-) pair photoproduction at mid-rapidity in ultra-peripheral Pb-Pb collisions at root s(NN)=2.76 TeV"

Abbas, E.; Abelev, B.; Adam, J.; Adamova, D.; Adare, A. M.; **Dash, A.*; Takahashi, J.***; et al.
ALICE Collaboration

The ALICE Collaboration at the LHC has measured the J/psi and psi' photoproduction at mid-rapidity in ultra-peripheral Pb-Pb collisions at root s(NN) = 2.76 TeV. The charmonium is identified via its leptonic decay for events where the hadronic activity is required to be minimal. The analysis is based on an event sample corresponding to an integrated luminosity of about 23 mu b(-1). The cross section for coherent and incoherent J/psi production in the rapidity interval -0.9 < y < 0.9, are d sigma(coh)(J/psi)/dy = 2.38(-0.24)(+0.34)(sta + sys) mb and d sigma(inc)(J/psi)/dy = 0.98(-0.17)(+0.19)(sta + sys) mb and , respectively. The results are compared to theoretical models for J/psi production and the coherent cross section is found to be in good agreement with those models incorporating moderate nuclear gluon shadowing at Bjorken-x around 10(-3),

such as EPS09 parametrization. In addition the cross section for the process gamma gamma -> e(+) e(-) has been measured and found to be in agreement with models implementing QED at leading order.

European Physical Journal C 73[11], 2617, 2013. DOI: 10.1140/epjc/s10052-013-2617-1

[P015-2014] "Different routes to pressure-induced volume collapse transitions in gadolinium and terbium metals"

Fabbris, G.; Matsuoka, T.; Lim, J.; **Mardegan, J. R. L.*;** Shimizu, K.; Haskel, D.; Schilling, J. S.

The sudden decrease in molar volume exhibited by most lanthanides under high pressure is often attributed to changes in the degree of localization of their 4f electrons. We give evidence, based on electrical resistivity measurements of dilute Y(Gd) and Y(Tb) alloys to 120 GPa, that the volume collapse transitions in Gd and Tb metals have different origins, despite their being neighbors in the periodic table. Remarkably, the change under pressure in the magnetic state of isolated Pr or Tb impurity ions in the nonmagnetic Y host appears to closely mirror corresponding changes in pure Pr or Tb metals. The collapse in Tb appears to be driven by an enhanced negative exchange interaction between 4f and conduction electrons under pressure (Kondo resonance) which, in the case of Y(Tb), dramatically alters the superconducting properties of the Y host, much like previously found for Y(Pr). In Gd, our resistivity measurements suggest that a Kondo resonance is not the main driver for its volume collapse. X-ray absorption and emission spectroscopies clearly show that 4f local moments remain largely intact across both volume collapse transitions ruling out 4f band formation (delocalization) and valence transition models as possible drivers. The results highlight the richness of behavior behind the volume collapse transition in lanthanides and demonstrate the stability of the 4f level against band formation to extreme pressure.

Physical Review B 88[24], 245103, 2013. DOI: 10.1103/PhysRevB.88.245103

[P016-2014] "Directed Flow of Charged Particles at Midrapidity Relative to the Spectator Plane in Pb-Pb Collisions at root s(NN)=2.76TeV"

Abelev, B.; Abelev, B.; Adam, J.; Adamova, D.; Adare, A. M.; **Dash, A.*; Takahashi, J.***; et al.
ALICE Collaboration

The directed flow of charged particles at midrapidity is measured in Pb-Pb collisions at root s(NN) p 2: 76 TeV relative to the collision symmetry plane defined by the spectator nucleons. A negative slope of the rapidity-odd directed flow component with approximately 3 times smaller magnitude than found at the highest RHIC energy is observed. This suggests a smaller longitudinal tilt of the initial system and disfavors the strong fireball rotation predicted for the LHC energies. The rapidity-even directed flow component is measured for the first time with spectators and found to be independent of pseudorapidity with a sign change at transverse momenta p(T) between 1.2 and 1: 7 GeV/c. Combined with the observation of a vanishing rapidity-even p(T) shift along the spectator deflection this is strong evidence for dipolelike initial density fluctuations in the overlap zone of the nuclei. Similar trends in the rapidity-even directed flow and the estimate from two-particle correlations at midrapidity, which is larger by about a factor of 40, indicate a weak correlation between fluctuating participant and spectator symmetry planes. These observations open new possibilities for investigation of the initial conditions in heavy-ion collisions with spectator nucleons.

Physical Review Letters 111[23], 232302, 2013. DOI: 10.1103/PhysRevLett.111.232302

[P017-2014] "Dose point kernels in liquid water: An intra--comparison between GEANT4-DNA and a variety of Monte Carlo codes"

Champion, C.; Incerti, S.; Perrot, Y.; Delorme, R.; Bordage, M. C.; Bardies, M.; Mascialino, B.; Tran, H. N.; Ivanchenko, V.; **Bernal, M.***; Francis, Z.; Groetz, J. E.; Fromm, M.; Campos, L.

Modeling the radio-induced effects in biological medium still requires accurate physics models to describe the interactions induced by all the charged particles present in the irradiated medium in detail. These interactions include inelastic as well as elastic processes. To check the accuracy of the very low energy models recently implemented into the GEANT4 toolkit for modeling the electron slowing-down in liquid water, the simulation of electron dose point kernels remains the preferential test. In this context, we here report normalized radial dose profiles, for mono-energetic point sources, computed in liquid water by using the very low energy "GEANT4-DNA" physics processes available in the GEANT4 toolkit. In the present study, we report an extensive intra-comparison of profiles obtained by a large selection of existing and well-documented Monte-Carlo codes, namely, EGSnrc, PENELOPE, CPA100, FLUKA and MCNPX.

Applied Radiation And Isotopes 83[SI], 137-141, Parte B, 2014. DOI: 10.1016/j.apradiso.2013.01.037

[P018-2014] "Effect of Lipid Coating on the Interaction Between Silica Nanoparticles and Membranes"

Tada, D. B.; Suraniti, E.; Rossi, L. M.; **Leite, C. A. P.***; Oliveira, C. S.; Tumolo, T. C.; Calemczuk, R.; Livache, T.; Baptista, M. S.

Lipid coating is a method highly used to improve the biocompatibility of nanoparticles (NPs), even though its effect on the NP properties is still object of investigation. Herein, silica NPs containing methylene blue, which is a photosensitizer used in a variety of biomedical applications, were coated with a phospholipid bilayer. Regarding the photophysical properties, lipid-coating did not cause significant changes since bare and lipid-coated NPs presented very similar absorption spectra and generated singlet oxygen with similar efficiencies. However, NP interaction with cells and membrane mimics was totally different for bare and lipid-coated NPs. Lipid-coated NPs were distributed through the cell cytoplasm whereas bare NPs were detected only in some vacuolar regions within the cells. Since cellular uptake and cytolocalization are influenced by NP adsorption on cell membranes, the interaction of lipid-coated and bare NPs were studied on a membrane mimic, i.e., Hybrid Bilayer Membranes (HBMs) made of different compositions of negatively charged and neutral lipids. Interactions of bare and lipid-coated NPs with HBMs were analyzed by Surface Plasmon Resonance Imaging. Bare NPs presented high adsorption and aggregation on HBMs independently of the surface charge. Conversely, lipid-coated NPs presented less aggregation on the membrane surface and the adsorption was dependent on the charges of the NPs and of the HBMs. Our results indicated that NPs aggregation on the membrane surface can be modulated by lipid coating, which affects the cytosolic distribution of the NPs.

Journal Of Biomedical Nanotechnology 10[3], 519-528, 2014. DOI: 10.1166/jbn.2014.1723

[P019-2014] "Elastic pp scattering from the optical point to past the dip: An empirical parametrization from ISR to the LHC"

Fagundes, D. A.*; Pancheri, G.; Grau, A.; Pacetti, S.; Srivastava, Y. N.

We describe the main features of recent LHC data on elastic pp scattering through a simple parametrization to the amplitude, inspired by a model proposed by Barger and Phillips in 1973, comprised of two exponentials with a relative phase. Despite its simplicity, this parametrization reproduces two essential aspects of the elastic differential cross section: the well-known precipitous descent in the forward direction and a sharp "dip'' structure. To include a complete description of data sets near -t =0 lecting the proton form factor. We find good descriptions of LHC7 and ISR data in either case. The form-factor model allows simple predictions for higher energies through asymptotic theorems and asymptotic sum rules in impact parameter space. We present predictions for this model at higher LHC energies, which can be used to test whether asymptotia is reached. The black-disk limit in this model is seen to be reached only for root S 10(6) TeV.

Physical Review D 88[9], 094019, 2013. DOI: 10.1103/PhysRevD.88.094019

[P020-2014] "Electrical resistivity under extreme conditions in the Ce3Ir4Sn13 heavy fermion compound"

Collave, J. R.; Borges, H. A.; Ramos, S. M.; Hering, E. N.; Fontes, M. B.; Baggio-Saitovitch, E.; Eichler, A.; Bittar, E. M.; **Pagliuso, P. G.***

We have performed measurements of temperature dependent electrical resistivity rho(T) under pressures up to 27 kbar and down to 0.1 K on single crystals of the Ce3Ir4Sn13 heavy fermion compound. At ambient pressure (P=0) we have identified in the rho(T) data interesting features associated with the presence of crystalline field effects, magnetic correlations, Kondo single impurity scattering and, possibly, a low temperature structural phase transition. All these features were mapped as a function of pressure which allowed us to construct a pressure-temperature phase diagram with these temperature scales. We have also carried out measurements of rho(T) as a function of magnetic fields up to H=8 T and the important temperature scales in rho(T) were followed with field. Enlightened also by temperature dependent specific heat experiments we discuss the possible microscopic origins of the features found in our rho(T) data.

Solid State Communications 177, 132-135, 2014. DOI: 10.1016/j.ssc.2013.10.015

[P021-2014] "Electron spin resonance of the half-Heusler antiferromagnet GdPdBi"

Jesus, C. B. R.*; Rosa, P. F. S.*; Garitezi, T. M.*; Lesseux, G. G.*; Urbano, R. R.*; Rettori, C.*; Pagliuso, P. G.*

We present electron spin resonance (ESR) measurements at X-Band frequency (nu=9.5 GHz) in powdered single crystal of the half-Heusler antiferromagnet GdPdBi grown using a Bi-flux method. In the paramagnetic state, a single Gd3+ Dysonian ESR line is observed with a nearly temperature independent g-factor of 1.99(2). On the other hand, the ESR linewidth Delta H increases non-linearly with decreasing temperature, indicating that the dominant relaxation mechanism occurs via Gd3+ spin-spin interaction. Approaching the AFM transition at T-N approximate to 13 K, the Gd3+ ESR line shifts to higher fields due to the emergence of short-range AFM correlations. Complementary data from macroscopic measurements such as magnetic susceptibility, heat capacity and electrical resistivity measurements provide further details about the global macroscopic physical properties of the GdPdBi compound.

Solid State Communications 177, 95-97, 2014. DOI: 10.1016/j.ssc.2013.09.033

[P022-2014] "Evidence of new magnetic ordering at high temperatures in Pb-based multiferroics perovskites"

Fraygola, B.; Nascimento, W. J.; **Coelho, A. A.*;** Garcia, D.; Eiras, J. A.

Presented here are the results of magnetic data that reveal that both Pb-based perovskites samples, Pb(Fe1/2Nb1/2)O-3 (lead iron niobate - PFN) and Pb(Fe2/3W1/3)O-3 (lead iron tungstate - PFW), exhibit a change in magnetic ordering from paramagnetic (PM) to weak ferromagnetic state at high temperature: a weak ferromagnetic order occurs in the samples around 530K. The experimental results suggest a possible involvement of the Pb ions into the superexchange of antiferromagnetic (AFM) phase.

Physica Status Solidi A-Applications And Materials Science 210[9], 1856-1860, 2013. DOI: 10.1002/pssa.201329011

[P023-2014] "Experimental study of unconfined surface wave discharges at atmospheric pressure by optical emission spectroscopy"

Ridenti, M. A.*; Souza-Correa, J. A.; **Amorim, J.***

A surface wave discharge (SWD) in argon at atmospheric pressure generated by a surfatron device was studied by optical emission spectroscopy (OES). Two distinct situations were investigated; (i) a discharge plasma in open air and (ii) a discharge plasma totally confined in a quartz tube. The electron density ne, electron temperature T-e and gas temperature T-g were investigated as a function of applied power and gas flow rate. The self-absorbing method was used to estimate the population of the metastable state Ar(1s(5)). These physical quantities were determined through optical measurements along the plasma axis of symmetry. The profile of the electron density presented a maximum value under certain conditions, in contrast with typical electron density profiles of SWDs which are usually monotonically decreasing. A correlation between the electron density and the metastable state Ar(1s(5)) was found in one of these cases, suggesting that stepwise ionization from metastable states and non-local kinetics play an important role on the unexpected increase in ionization degree along the discharge.

Journal Of Physics D-Applied Physics 47[4], 045204, 2014. DOI: 10.1088/0022-3727/47/4/045204

[P024-2014] "Fabrication of p-type silicon nanowires for 3D FETs using focused ion beam"

dos Santos, M. V. P.*; Lima, L. P. B.; Diniz, J. A.; Godoy, J.

A Ga+ focused ion beam (GaFIB) from a FIB/scanning electron microscopy (SEM) dual beam system was used for Si milling and p-type local doping of p+-type silicon nanowires (p+-SiNWs). The resulting p+-SiNWs were then used to create pMOS junctionless nanowire transistor (INT) prototypes for silicon-on-insulator wafer substrates. The electron beam from the FIB/SEM dual beam system was used to deposit SiO2 gate dielectric and Pt source/drain electrodes for JNT transistors. Width, length, and height dimensions of p+-SiNWs were approximately 35 nm, 6 mu m, and 15 nm, respectively, and the JNT gate length was 1 mu m. Finally, photolithography, Al sputtering deposition, and lift-off processing were conducted to define the Al gate electrode and contacts on Pt source/drain electrodes. Energy dispersive x-ray spectroscopy measurements were taken to confirm the surface composition of p+-SiNWs and Ga doping. Drain-source current (I-DS) versus drain-source voltage (V-DS) measurements of JNT transistors indicated that the device is working like a JNT device (gated resistor). The authors noted high resistance on Al/Pt source and drain electrodes, which leads to distortions on Ins versus V-DS curves as non-ohmic electrical contact for low V-DS signal.

However, these distortions can be reduced with a longer contact sintering process or by increased p+-SiNW doping. Our conclusions indicate that utilizing a GaFIB/SEM dual beam system for Si milling, Ga doping, and SiO2 and Pt depositions can be a favorable alternative for fabricating junctionless devices based on p+-SiNWs.

Journal Of Vacuum Science & Technology B 31[6], 06FA01, 2013. DOI: 10.1116/1.4823763

[P025-2014] "Floating liquid bridge tensile behavior: Electric-field-induced Young's modulus measurements"

Teschke, O.*; Soares, D. M.*; Valente, J. F.*

A floating bridge is formed spontaneously when high voltage is applied to polar fluids in two capillary tubes that were in contact and then separated. This bridge bends under its own weight, and its bending profile was used to calculate its Young's modulus. For electric field intensities of similar to 10(6) V/m, water bridges exhibit viscoelastic behavior, with Young's moduli of similar to 24MPa; dimethylsulfoxide (DMSO) bridges exhibited Young's moduli of similar to 60 kPa. The scheme devised to measure the voltage drop across the water bridge for high voltages applied between the electrodes shows that the bulk water resistance decreases with increasing voltage.

Applied Physics Letters 103[25], 251608, 2013. DOI: 10.1063/1.4853955

[P026-2014] "FT-IR and Raman spectra and DFT calculations on bis(L-histidinato)nickel(II) monohydrate"

Maia, J. R.; Lima, J. A., Jr.; Freire, P. T. C.; Mendes, J.; Nogueira, C. E. S.; Teixeira, A. M. R.; de Menezes, A. S.; Remedios, C. M. R.; **Cardoso, L. P.***

In this work the Fourier transform infrared and the Raman spectra of bis(L-hisidinato)nickel(II) monohydrate were recorded at room temperature. Optimized geometry and vibrational frequencies were obtained by means of Density Functional Theory (DFT). Experimental and theoretical vibrational spectra were compared and a complete analysis of the modes was done in terms of the Potential Energy Distribution (PED).

Journal Of Molecular Structure 1054, 143-149, 2013. DOI: 10.1016/j.molstruc.2013.09.042

[P027-2014] "Hardfats as crystallization modifiers of cocoa butter"

Ribeiro, A. P. B.; Basso, R. C.; dos Santos, A. O.; **Andrade, G. C.*; Cardoso, L. P.***; Kieckbusch, T. G.

Hardfats, or fully hydrogenated oils, consist of materials with homogeneous composition, composed of high melting point triacylglycerol. Hardfats are regarded as relatively new materials, and remain unexplored in lipid technology, notwithstanding being low-cost industrial products. They can behave as modulators of the crystallization process, acting as preferential nuclei for ordering the crystal lattice and inducing specific polymorphic habits, with great potential for use in crystallization processes. This work evaluated the influence of the addition of different hardfats on the crystallization patterns of cocoa butter (CB). Fully hydrogenated oils with significantly different chemical composition, obtained from palm kernel oil (FHPKO), palm oil (FHPO), cottonseed oil (FHCO), soybean oil (FHSO), and crambe oil (FHCrO), were considered. Blends of CB/hardfats, at concentrations of 1%, 3%, and 5% (by weight) were produced and the crystallization isotherms, thermal behavior, and polymorphism determined. Hardfats FHPO, FHCO, FHSO, and FHCrO proved to be effective additives to modulate the crystallization characteristics of CB, in respect to crystallization kinetics and thermal behavior. Only the hardfat from crambe oil, FHCrO, presented stabilizing effect on the polymorphism of CB, delaying the transition VVI. Practical applications: The use of hardfats as crystallization additives in products containing CB, for technological adjustment of CB formulations in order to harmonize events like solidification kinetics, thermal behavior, and polymorphism. Hardfats may act as potential modulators of CB crystallization, with the purpose to obtain higher quality products at significantly reduced cost in industrial processing.

European Journal Of Lipid Science And Technology 115[12], SI, 1462-1473, 2013. DOI: 10.1002/ejlt.201300052

[P028-2014] "Hot Brownian carriers in the Langevin picture: Application to a simple model for the Gunn effect in GaAs"

Bauke, F. C.*; Lagos, R. E.

We consider a charged Brownian gas under the influence of external, static and uniform electric and magnetic fields, immersed in a uniform bath temperature. We obtain the solution for the associated Langevin equation, and thereafter the evolution of the nonequilibrium temperature towards a nonequilibrium (hot) steady state. We apply our results to a simple yet relevant Brownian model for carrier transport in GaAs. We obtain a negative differential conductivity regime (Gunn effect) and discuss and compare our results with the experimental results.

Physica A-Statistical Mechanics And Its Applications 393, 235-243, 2014. DOI: 10.1016/j.physa.2013.08.081

[P029-2014] "Identifying clouds over the Pierre Auger Observatory using infrared satellite data"

Abreu, P.; Aglietta, M.; **Chinellato, J. A.*; Daniel, B.*; de Mello, W. J. M.*, Jr.; Dobrigkeit, C.*; Escobar, C. O.*; Fauth, A. C.*; Goncalves, P.*; Kemp, E.*; Muller, M. A.*; Pakk Selmi-Dei, D.*; Zimbres Silva, M.*;** et al.
Pierre Auger Collaboration

We describe a new method of identifying night-time clouds over the Pierre Auger Observatory using infrared data from the Imager instruments on the GOES-12 and GOES-13 satellites. We compare cloud. identifications resulting from our method to those obtained by the Central Laser Facility of the Auger Observatory. Using our new method we can now develop cloud probability maps for the 3000 km(2) of the Pierre Auger Observatory twice per hour with a spatial resolution of similar to 2.4 km by similar to 5.5 km. Our method could also be applied to monitor cloud cover for other ground-based observatories and for space-based observatories.

Astroparticle Physics [50-52], 92-101, 2013. DOI: 10.1016/j.astropartphys.2013.09.004

[P030-2014] "Intraband absorption in GaAs-(Ga,Al) As variably spaced semiconductor superlattices under crossed electric and magnetic fields"

Reyes-Gomez, E.; Raigoza, N.; **Oliveira, L. E.***

A theoretical study of the intraband absorption properties of GaAs-Ga1-xAlxAs variably spaced semiconductor superlattices under crossed magnetic and electric fields is presented.

Calculations are performed for the applied electric field along the growth-axis direction, whereas the magnetic field is considered parallel to the heterostructure layers. By defining a critical electric field so that the heterostructure energy levels are aligned in the absence of the applied magnetic fields, one finds that, in the weak magnetic-field regime, an abrupt red shift of the absorption coefficient maxima is obtained at fields equal to or larger than the critical electric field, a fact which may be explained from the localization properties of the electron wave functions. Results in the strong magnetic-field regime reveal a rich structure on the intraband absorption coefficient which may be explained from the strong dispersion exhibited by both the energy levels and transition strengths as functions of the generalized orbit-center position. Moreover, the possibility of occurrence of absorption in a wide frequency range is also demonstrated. Present calculated results may be of interest for future design and improvement of multilayered-based photovoltaic and solar-cell devices.

EPL 104[4], 47008, 2013. DOI: 10.1209/0295-5075/104/47008

[P031-2014] "Jet and underlying event properties as a function of charged-particle multiplicity in proton-proton collisions at root s=7 TeV"

Chatrchyan, S.; Khachatryan, V.; Sirunyan, A. M.; Tumasyan, A.; **Chinellato, J.*; Manganote, E. J. Tonelli*;** et al.
CMS Collaboration

Characteristics of multi-particle production in proton-proton collisions at root s = 7 TeV are studied as a function of the charged-particle multiplicity, N (ch). The produced particles are separated into two classes: those belonging to jets and those belonging to the underlying event. Charged particles are measured with pseudorapidity |eta|< 2.4 and transverse momentum p (T)> 0.25 GeV/c. Jets are reconstructed from charged-particles only and required to have p (T)> 5 GeV/c. The distributions of jet p (T), average p (T) of charged particles belonging to the underlying event or to jets, jet rates, and jet shapes are presented as functions of N (ch) and compared to the predictions of the pythia and herwig event generators. Predictions without multi-parton interactions fail completely to describe the N (ch)-dependence observed in the data. For increasing N (ch), pythia systematically predicts higher jet rates and harder p (T) spectra than seen in the data, whereas herwig shows the opposite trends. At the highest multiplicity, the data-model agreement is worse for most observables, indicating the need for further tuning and/or new model ingredients.

European Physical Journal C 73[12], 2674, 2013. DOI: 10.1140/epjc/s10052-013-2674-5

[P032-2014] "K-S(0) and Lambda Production in Pb-Pb Collisions at root s(NN)=2: 76 TeV"

Abbas, E.; Abelev, B.; Adam, J.; Adamova, D.; Adare, A. M.; **Dash, A.*; Takahashi, J.***; et al.
ALICE Collaboration

The ALICE measurement of K-S(0) and Lambda production at midrapidity in Pb-Pb collisions at root sNN = 2.76 TeV is presented. The transverse momentum (p(T)) spectra are shown for several collision centrality intervals and in the p(T) range from 0: 4 GeV/c (0: 6 GeV/c for Lambda) to 12 GeV/c. The p(T) dependence of the Lambda/K-S(0) ratios exhibits maxima in the vicinity of 3 GeV/c, and the positions of the maxima shift towards higher p(T) with increasing collision centrality. The magnitude of these maxima increases by almost a factor of three between most peripheral and most central Pb-Pb collisions. This baryon excess at intermediate p(T) is not observed in pp interactions at root s = 0.9 TeV and at root s = 7 TeV. Qualitatively, the baryon enhancement in heavy-ion collisions is expected from radial flow. However, the measured p(T) spectra above 2 GeV/c progressively decouple from hydrodynamical-model calculations. For higher values of p(T), models that incorporate the influence of the medium on the fragmentation and hadronization processes describe qualitatively the p(T) dependence of the Lambda/K-S(0) ratio.

Physical Review Letters 111[22], 222301, 2013. DOI: 10.1103/PhysRevLett.111.222301

[P033-2014] "Lattice strain distribution resolved by X-ray Bragg-surface diffraction in an Si matrix distorted by embedded FeSi2 nanoparticles"

Lang, R.; de Menezes, A. S.; dos Santos, A. O.; **Reboh, S.***; Meneses, E. A.; Amaral, L.; **Cardoso, L. P.***

Out-of-plane and primarily in-plane lattice strain distributions, along the two perpendicular crystallographic directions on the subsurface of a silicon layer with embedded FeSi2 nanoparticles, were analyzed and resolved as a function of the synchrotron X-ray beam energy by using omega:phi mappings of the (111) and (111) Bragg-surface diffraction peaks. The nanoparticles, synthesized by ion-beam-induced epitaxial crystallization of Fe+-implanted Si(001), were observed to have different orientations and morphologies (sphere-and plate-like nanoparticles) within the implanted/recrystallized region. The results show that the shape of the synthesized material singularly affects the surrounding Si lattice. The lattice strain distribution elucidated by the nonconventional X--ray Bragg-surface diffraction technique clearly exhibits an anisotropic effect, predominantly caused by plate-shaped nanoparticles. This type of refined detection reflects a key application of the method, which could be used to allow discrimination of strains in distorted semiconductor substrate layers.

Journal Of Applied Crystallography 46, 1796-1804, Parte 6, 2013. DOI: 10.1107/S0021889813026046

[P034-2014] "Lithium-doped endohedral single-walled carbon nanotubes can arise during tube growth"

Matsubara, E. Y.; **Luengo, C. A.***; Rosolen, J. M.

This Letter shows that it is possible to dope single-walled carbon nanotubes (SWCNT) with lithium during SWCNT growth in an arc reactor. Depending on the oxygen and lithium concentrations in the reactor, one can obtain endohedral Li@ SWCNT after rinsing the product in water. Oxygen plays a decisive role in Li insertion during SWCNT growth and in the diameter distribution of the samples. Doping the tubes with Li produces end-closed SWCNT bundles that afford more stable dispersion in water as compared with non-doped tubes.

Chemical Physics Letters 590, 175-179, 2013. DOI: 10.1016/j.cplett.2013.10.077

[P035-2014] "Long-range angular correlations of pi, K and p in p-Pb collisions at root s(NN)=5.02 TeV"

Abbas, E.; Abelev, B.; Adam, J.; Adamova, D.; Adare, A. M.; **Dash, A.*; Takahashi, J.*;** et al.
ALICE Collaborat

Angular correlations between unidentified charged trigger particles and various species of charged associated particles (unidentified particles, pions, kaons, protons and antiprotons) are measured by the ALICE detector in p-Pb collisions at a nucleon-nucleon centre-of-mass energy of 5.02 TeV in the transverse-momentum range 0.3 < p(T) < 4 GeV/c.

The correlations expressed as associated yield per trigger particle are obtained in the pseudorapidity range vertical bar n(lab)vertical bar < 0.8. Fourier coefficients are extracted from the long-range correlations projected onto the azimuthal angle difference and studied as a function of p(T) and in intervals of event multiplicity. In high-multiplicity events, the second--order coefficient for protons, 4, is observed to be smaller than that for pions, v(2)(pi), up to about p(T) = 2 GeV/c. To reduce correlations due to jets, the per-trigger yield measured in low--multiplicity events is subtracted from that in high-multiplicity events. A two-ridge structure is obtained for all particle species. The Fourier decomposition of this structure shows that the second-order coefficients for pions and kaons are similar. The v(2)(p) is found to be smaller at low P-T and larger at higher p(T) than v(2)(pi), with a crossing occurring at about 2 GeV/c. This is qualitatively similar to the elliptic-flow pattern observed in heavy-ion collisions. A mass ordering effect at low transverse momenta is consistent with expectations from hydrodynamic model calculations assuming a collectively expanding system.

Physics Letters B 726[1-3], 164-177, 2013. DOI: 10.1016/j.physletb.2013.08.024

[P036-2014] "Low temperature properties of winterized methyl babassu biodiesel"

Silva, M. C. D.; da Silva, L. M.; Brando, K. S.; Souza, A. G.; **Cardoso, L. P.***; dos Santos, A. O.

In this work, differential scanning calorimetry and X-ray diffraction techniques were employed to evaluate the influence of the winterization process on the low temperature properties of methyl babassu biodiesel. The results have shown that the crystallization onset temperature for the non-winterized biodiesel is around 266.4 K (-6.6 A degrees C) which is reduced to 263.6 K (-9.4 A degrees C) for the liquid fraction of winterized biodiesel. The 14 % reduction in the amount of saturated fatty acid methyl esters is probably responsible for the improvement of low temperature properties of winterized methyl babassu biodiesel.

Journal Of Thermal Analysis And Calorimetry 115[1], 635-640, 2014. DOI: 10.1007/s10973-013-3263-4

[P037-2014] "Magnetic ordering in nickel-zinc nanoferrite thin film formed by Langmuir Blodgett technique"

Thakur, S.; Pandit, P.; **Sharma, S. K.***; Katyal, S. C.; Singh, M.; Gupta, A.

Nickel-zinc nanoferrite thin films, which reveal application for magnetic materials, were prepared by Langmuir-Blodgett technique. X-ray reflectivity fitting was done using three layer model. Thickness of a monolayer of nanoparticles is obtained as 23.5 angstrom. Surface roughness increases as the thickness of the film increases. Fourier transform infrared spectra confirmed that the structure remains cubic spinel after thin film formation. We have measured zero-field cooled and field cooled magnetization and discussed the behavior in three parts: the ferromagnetic part, transition region, and the superparamagnetic part.

Applied Physics Letters 103[23], 233102, 2013. DOI: 10.1063/1.4837735

[P038-2014] "Magnetic Polarization of the Tunneling Current"

Fernandes, I. L.*; Cabrera, G. G.*

In this work, we theoretically study the spin-dependent transport in a magnetic tunnel junction (MTJ). Using a simple model and ballistic transport, the magnetic polarization of the tunneling current on this system is studied by focusing on the tunneling of s and d electrons. We investigate the tunneling of these electrons through potential barriers, which represents the insulating layer between the ferromagnetic electrodes. We also examine how the conductance depends on voltage applied between the electrodes and on the effective mass of the electrons. The conductance is controlled by the transmission coefficient of the tunnel effect, and qualitatively it is known that tunneling probability of the electrons is lower than the electrons. We also estimate the effect of the tunneling magnetoresistance (TMR) and it is strongly influenced by the effective mass of the electrons. The electrons do not contribute significantly to the TMR.

IEEE Transactions On Magnetics 49[12], 5635-5638, 2013. DOI: 10.1109/TMAG.2013.2272214

[P039-2014] "Measurement of the cross section and angular correlations for associated production of a Z boson with b hadrons in pp collisions at root s=7 TeV"

Chatrchyan, S.; Khachatryan, V.; Sirunyan, A. M.; Tumasyan, A. ; **Chinellato, J.*; Manganote, E. J. Tonelli***; et al.
CMS Collaboration

A study of proton-proton collisions in which two b hadrons are produced in association with a Z boson is reported. The collisions were recorded at a centre-of-mass energy of 7 TeVwith the CMS detector at the LHC, for an integrated luminosity of 5.2 fb(-1). The b hadrons are identified by means of displaced secondary vertices, without the use of reconstructed jets, permitting the study of b-hadron pair production at small angular separation. Differential cross sections are presented as a function of the angular separation of the b hadrons and the Z boson. In addition, inclusive measurements are presented. For both the inclusive and differential studies, different ranges of Z boson momentum are considered, and each measurement is compared to the predictions from different event generators at leading-order and next-to-leading-order accuracy.

Journal Of High Energy Physics 12, 039, 2013. DOI: 10.1007/JHEP12(2013)039

[P040-2014] "Measurement of the differential and double--differential Drell-Yan cross sections in proton-proton collisions at root s=7 TeV"

Chatrchyan, S.; Khachatryan, V.; Sirunyan, A. M.; Tumasyan, A.; **Chinellato, J.*; Manganote, E. J. Tonelli*;** et al.
CMS Collaboration

Measurements of the differential and double-differential Drell--Yan cross sections are presented using an integrated luminosity of 4.5 (4.8) fb(-1) in the dimuon (dielectron) channel of proton-proton collision data recorded with the CMS detector at the LHC at = 7 TeV. The measured inclusive cross section in the Z-peak region (60-120 GeV) is sigma(a""a"") = 986.4 +/- 0.6 (stat.) +/- 5.9 (exp. syst.) +/- 21.7 (th. syst.) +/- 21.7 (lum.) pb for the combination of the dimuon and dielectron channels. Differential cross sections d sigma/dm for the dimuon, dielectron, and combined channels are measured in the mass range 15 to 1500 GeV and corrected to the full phase space. Results are also presented for the measurement of the double-differential cross section d(2)sigma/dm d|y| in the dimuon channel over the mass range 20 to 1500 GeV and absolute dimuon rapidity from 0 to 2.4. These measurements are compared to the predictions of perturbative QCD calculations at next-to-leading and next-to-next-to-leading orders using various sets of parton distribution functions.

Journal Of High Energy Physics 12, 030, 2013. DOI: 10.1007/JHEP12(2013)030

[P041-2014] "Measurement of the prompt J/psi and psi(2S) polarizations in pp collisions at root s=7 TeV"

Chatrchyan, S.; Khachatryan, V.; Sirunyan, A. M.; Tumasyan, A.; **Chinellato, J.*; Manganote, E. J. Tonelli***; et al.
CMS Collaboration

The polarizations of prompt J/psi and psi(2S) mesons are measured in proton-proton collisions at root s = 7 TeV, using a dimuon data sample collected by the CMS experiment at the LHC, corresponding to an integrated luminosity of 4.9 fb(-1). The prompt J/psi and psi(2S) polarization parameters lambda, lambda, and lambda, as well as the frame-invariant quantity (lambda) over bar. are measured from the dimuon decay angular distributions in three different polarization frames. The J/psi results are obtained in the transverse momentum range 14 < P-T < 70 GeV, in the rapidity intervals |y| < 0.6 and 0.6 < |y| < 1.2. The corresponding psi(2S) results cover 14 < PT < 50 GeV and include a third rapidity bin, 1.2 < |y| < 1.5. No evidence of large polarizations is seen in these kinematic regions, which extend much beyond those previously explored.

Physics Letters B 727[4-5], 381-402, 2013. DOI: 10.1016/j.physletb.2013.10.055

[P042-2014] "Minkowski structure for purity and entanglement of Gaussian bipartite states"

de Oliveira, M. C.*; Nicacio, F.*; Mizrahi, S. S.

The relation between the symplectic and Lorentz groups is explored to investigate entanglement features in a two-mode bipartite Gaussian state. We verify that the correlation matrix of arbitrary Gaussian states can be associated with a hyperbolic space with a Minkowski metric, which is divided in two regions: separabilitylike and entanglementlike, in equivalence to timelike and spacelike in special relativity. This correspondence naturally allows the definition of two insightful invariant squared distance measures: one related to the purity and another related to amount of entanglement. The second distance allows us to define a measure for entanglement in terms of the invariant interval between the given state and its closest separable state, given in a natural manner without the requirement of a minimization procedure.

Physical Review A 88[5], 052324, 2013. DOI: 10.1103/PhysRevA.88.052324

[P043-2014] Multiplicity dependence of the average transverse momentum in pp, p-Pb, and Pb-Pb collisions at the LHC

Abbas, E.; Abelev, B.; Adam, J.; Adamova, D.; Adare, A. M.; **Dash, A.*; Takahashi, J.*; et al.**
ALICE Collaboration

The average transverse momentum (p(T)) versus the charged--particle multiplicity N-ch was measured in p-Pb collisions at a collision energy per nucleon-nucleon root S-NN = 5.02 TeV and in pp collisions at collision energies of root s = 0.9, 2.76, and 7 TeV in the kinematic range 0.15 < p(T) < 10.0 GeV/c and vertical bar eta vertical bar < 0.3 with the ALICE apparatus at the LHC. These data are compared to results in Pb-Pb collisions at root S-NN = 2.76 TeV at similar charged-particle multiplicities. In pp and p-Pb collisions, a strong increase of (p(T)) with N-ch is observed, which is much stronger than that measured in Pb-Pb collisions. For pp collisions, this could be attributed, within a model of hadronizing strings, to multiple--parton interactions and to a final-state color reconnection mechanism. The data in p-Pb and Pb-Pb collisions cannot be described by an incoherent superposition of nucleon-nucleon collisions and pose a challenge to most of the event generators.

Physics Letters B 727[4-5], 371-380, 2013. DOI: 10.1016/j.physletb.2013.10.054

[P044-2014] "Neutrinos from collapsars"

Vieyro, F. L.*; Romero, G. E.; **Peres, O. L. G.***

Context. Long gamma-ray bursts (GRBs) are associated with the gravitational collapse of very massive stars. The central engine of a GRB can collimate relativistic jets that propagate inside the stellar envelope. The shock waves produced when the jet disrupts the stellar surface are capable of accelerating particles up to very high energies. Aims. If the jet has hadronic content, neutrinos will be produced via charged pion decays. The main goal of this work is to estimate the neutrino emission produced in the region close to the surface of the star, taking pion and muon cooling into account, along with subtle effects arising from neutrino production in a highly magnetized medium. Methods. We estimate the maximum energies of the different kinds of particles and solve the coupled transport equations for each species. Once the particle distributions are known, we calculate the intensity of neutrinos. We study the different effects on the neutrinos that can change the relative weight of different flavors. In particular, we consider the effects of neutrino oscillations, and of neutrino spin precession caused by strong magnetic fields. Results. The expected neutrino signals from the shocks in the uncorking regions of Population III events is very weak, but the neutrino signal produced by Wolf-Rayet GRBs with z < 0.5 is not far from the level of the atmospheric background. Conclusions. The IceCube experiment does not have the sensitivity to detect neutrinos from the implosion of the earliest stars, but a number of high-energy neutrinos may be detected from nearby long GRBs. The cumulative signal should be detectable over several years (similar to 10 yr) of integration with the full 86-string configuration.

Astronomy & Astrophysics 558, UNSP A142, 2013. DOI: 10.1051/0004-6361/201321701

[P045-2014] "Novel calibration for LA-ICP-MS-based fission--track thermochronology"

Soares, C. J.; **Guedes, S.*; Hadler, J. C.***; Mertz-Kraus, R.; Zack, T.; **Iunes, P. J.***

We present a novel age-equation calibration for fission-track age determinations by laser ablation inductively coupled plasma mass spectrometry. This new calibration incorporates the efficiency factor of an internal surface, [eta q](is), which is obtained by measuring the projected fission-track length, allowing the determination of FT ages directly using the recommended spontaneous fission decay constant. Also, the uranium concentrations in apatite samples are determined using a Durango (Dur-2, 7.44 mu g/g U) crystal and a Mud Tank (MT-7, 6.88 mu g/g U) crystal as uranium reference materials. The use of matrix-matched reference materials allows a reduction in the uncertainty of the uranium measurements to those related to counting statistics, which are ca. 1 % taking into account that no extra source of uncertainty has to be considered. The equations as well as the matrix--matched reference materials are evaluated using well-dated samples from Durango, Fish Canyon Tuff, and Limberg as unknown samples. The results compare well with their respective published ages determined through other dating methods. Additionally, the results agree with traditional fission-track ages using both the zeta approach and the absolute approach, suggesting that the calibration presented in this work can be robustly applied in geological context. Furthermore, considering that fission-track ages can be determined without an age standard sample, the fission-track thermochronology approach presented here is assumed to be a valuable dating tool.

Physics And Chemistry Of Minerals 41[1], 65-73, 2014. DOI: 10.1007/s00269-013-0624-2

[P046-2014] "Optical Monitoring and Detection of Spinal Cord Ischemia"

Mesquita, R. C.*; D'Souza, A.; Bilfinger, T. V.; Galler, R. M.; Emanuel, A.; Schenkel, S. S.; Yodh, A. G.; Floyd, T. F.

Spinal cord ischemia can lead to paralysis or paraparesis, but if detected early it may be amenable to treatment. Current methods use evoked potentials for detection of spinal cord ischemia, a decades old technology whose warning signs are indirect and significantly delayed from the onset of ischemia. Here we introduce and demonstrate a prototype fiber optic device that directly measures spinal cord blood flow and oxygenation. This technical advance in neurological monitoring promises a new standard of care for detection of spinal cord ischemia and the opportunity for early intervention. We demonstrate the probe in an adult Dorset sheep model. Both open and percutaneous approaches were evaluated during pharmacologic, physiological, and mechanical interventions designed to induce variations in spinal cord blood flow and oxygenation. The induced variations were rapidly and reproducibly detected, demonstrating direct measurement of spinal cord ischemia in real-time. In the future, this form of hemodynamic spinal cord diagnosis could significantly improve monitoring and management in a broad range of patients, including those undergoing thoracic and abdominal aortic revascularization, spine stabilization procedures for scoliosis and trauma, spinal cord tumor resection, and those requiring management of spinal cord injury in intensive care settings.

Plos One 8[12], e83370, 2013. DOI: 10.1371/journal.pone.0083370

[P047-2014] "Optical properties of two-dimensional metamaterial photonic crystals"

Mejia-Salazar, J. R.*

In the present work, we theoretically study a 2D photonic crystal (PC) comprised by double negative (DNG) metamaterial cylinders, showing that such a system presents a superior light-matter interaction when compared with their single negative (SNG) plasmonic PC counterparts, suggesting a route to enhance the performance of sensors and photovoltaic cells. On the other hand, we have observed that depending on the frequency, the mode symmetry resembles either the case of SNG electric (SNG-E) or SNG magnetic (SNG-M) PC, suggesting that either the electric or magnetic character of the DNG metamaterial dominates in each case.

Journal Of Applied Physics 114[22], 223513, 2013. DOI: 10.1063/1.4847977

[P048-2014] "Performance of the ALICE VZERO system"

Abbas, E.; Abelev, B.; Adam, J.; Adamova, D.; Adare, A. M.; **Dash, A.*; Takahashi, J.*; et al.**
ALICE Collaboration

ALICE is an LHC experiment devoted to the study of strongly interacting matter in proton-proton, proton-nucleus and nucleus-nucleus collisions at ultra-relativistic energies. The ALICE VZERO system, made of two scintillator arrays at asymmetric positions, one on each side of the interaction point, plays a central role in ALICE. In addition to its core function as a trigger source, the VZERO system is used to monitor LHC beam conditions, to reject beam-induced backgrounds and to measure basic physics quantities such as luminosity, particle multiplicity, centrality and event plane direction in nucleus-nucleus collisions. After describing the VZERO system, this publication presents its performance over more than four years of operation at the LHC.

Journal Of Instrumentation 8[P10016], 2013. DOI: 10.1088/1748-0221/8/10/P10016

[P049-2014] "Phase space flow in the Husimi representation"

Veronez, M.*; de Aguiar, M. A. M.*

We derive a continuity equation for the Husimi function evolving under a general non-Hermitian Hamiltonian and identify the phase space flow associated with it. For the case of unitary evolution we obtain explicit formulas for the quantum flow, which can be written as a classical term plus quantum corrections. The quantum terms can be expanded in powers of Planck's constant providing a series of semiclassical corrections to the classical flow. We test the exact and semiclassical formulas for a particle in a double well potential and find numerical evidence that the zeros of the Husimi function are always saddle points of the flow. Merging or splitting of stagnation points, reported for the Wigner flow, was not observed.

Journal Of Physics A-Mathematical And Theoretical 46[48], 485304, 2013. DOI: 10.1088/1751-8113/46/48/485304

[P050-2014] "Phenomenology of MaVaN's Models in Reactor Neutrino Data"

Carneiro, M. F.*; de Holanda, P. C.*

Mass Varying Neutrinos (MaVaN's) mechanisms were proposed to link the neutrino mass scale with the dark energy density, addressing the coincidence problem. In some scenarios, this mass can present a dependence on the baryonic density felt by neutrinos, creating an effective neutrino mass that depends both on the neutrino and baryonic densities. In this work, we study the phenomenological consequence of MaVaN's scenarios in which the matter density dependence is induced by Yukawa interactions of a light neutral scalar particle which couples to neutrinos and matter. Under the assumption of one mass scale dominance, we perform an analysis of KamLAND neutrino data which depends on 4 parameters: the two standard oscillation parameters, Delta m(0,21)(2) and tan (2)theta(12), and two new coefficients which parameterize the environment dependence of neutrino mass. We introduce an Earth's crust model to compute precisely the density in each point along the neutrino trajectory. We show that this new description of density does not affect the analysis with the standard model case. With the MaVaN model, we observe a first order effect in lower density, which leads to an improvement on the data description.

Advances In High Energy Physics, 293425, 2013. DOI: 10.1155/2013/293425

[P051-2014] "Photo induced dissociation of amino acids free from thermal degradation effects: A case study applied to DL-Valine"

da Silva, A. M.; Mocellin, A.; Farrokhpour, H.; Mundim, M. S. P.; **de Brito, A. N.***

We present a careful study of the thermal degradation effects in the mass spectrum of DL-Valine using a quadrupole mass spectrometer and a time of flight - mass spectrometer. This allows setting the temperature of 95 +/- 10 C as threshold for the sublimation of our solid sample. Based on the assignments for each ionic fragment detected, it is possible to separate the mass peaks in groups,

explaining what are the principal bond breaks involved in the specific ionic yield, whose procedure can be extended to other amino acids.

Journal Of Electron Spectroscopy And Related Phenomena 189[SI], 56-60, 2013. DOI: 10.1016/j.elspec.2013.02.004

[P052-2014] "Probing dark energy through scale dependence"

Motta, M.*; Sawicki, I.; Saltas, I. D.; Amendola, L.; Kunz, M.

We consider the consequences of having no prior knowledge of the true dark energy model for the interpretation of cosmological observations. The magnitude of redshift-space distortions and weak-lensing shear is determined by the metric on the geodesics of which galaxies and light propagate. We show that, given precise enough observations, we can use these data to completely reconstruct the metric on our past light cone and therefore to measure the scale and time dependence of the anisotropic stress and the evolution of the gravitational potentials in a model-independent manner. Since both dark matter and dark energy affect the visible sector only through the gravitational field they produce, they are inseparable without a model for dark energy: galaxy bias cannot be measured and therefore the distribution of dark matter determined; the peculiar velocity of dark matter can be identified with that of the galaxies only when the equivalence principle holds. Given these limitations, we show how one can nonetheless build tests for classes of dark energy models which depend on making measurements at multiple scales at a particular redshift. They are null tests on the model-independent observables, do not require modeling evolution in time, and do not require any parametrization of the free functions of these models-such as the sound speed. We show that one in principle could rule out or constrain the whole class of the most general scalar--tensor theories even without assuming the quasistatic limit.

Physical Review D 88[12], 124035, 2013. DOI: 10.1103/PhysRevD.88.124035

[P053-2014] "Rapidity distributions in exclusive Z plus jet and gamma plus jet events in pp collisions at root s=7 TeV'

Chatrchyan, S.; Khachatryan, V.; Sirunyan, A. M.; Tumasyan, A.; **Chinellato, J.*; Tonelli Manganote, E. J.***; et al.
CMS Collaboration

Rapidity distributions are presented for events containing either a Z boson or a photon with a single jet in proton-proton collisions produced at the CERN LHC. The data, collected with the CMS detector at root s = 7 TeV, correspond to an integrated luminosity of 5.0 fb(-1). The individual rapidity distributions of the boson and the jet are consistent within 5% with expectations from perturbative QCD. However, QCD predictions for the sum and the difference in rapidities of the two final-state objects show discrepancies with CMS data. In particular, next-to-leading-order QCD calculations, and two common Monte Carlo event generators using different methods to match matrix-element partons with parton showers, appear inconsistent with the data as well as with each other.

Physical Review D 88[11], 112009, 2013. DOI: 10.1103/PhysRevD.88.112009

[P054-2014] "Restricting the LSND and MiniBooNE sterile neutrinos with the IceCube atmospheric neutrino data"

Esmaili, A.*; Smirnov, A. Y.

We study oscillations of the high energy atmospheric neutrinos in the Earth into sterile neutrinos with the eV-scale mass. The MSW resonance and parametric enhancement of the (nu) over bar (mu) -> (nu) over bar (s) oscillations lead to distortion of the zenith angle distribution of the muon-track events which can be observed by IceCube. Due to matter effect, the IceCube signal depends not only on the mixing element U-mu 4 relevant for LSND and MiniBooNE but also on U-tau 4 and the CP-violating phase delta(24). We show that the case with U-tau 4 = delta(24) = 0 leads to the weakest IceCube signal and therefore should be used to bound U-mu 4. We compute the zenith angle distributions of the nu(mu)-events for different energy intervals in the range (0.1 - 10) TeV and find that inclusion of the energy information (binning in energy) improves the sensitivity to nu(s) drastically. We estimate that with already collected (during 3 - 4 years) IceCube statistics the bound vertical bar U-mu 4 vertical bar(2) < 0.01 (99% C.L.) can be established and the mixing required by LSND and MiniBooNE can be excluded at (4-6)sigma confidence level.

Journal Of High Energy Physics [12], 014, 2013. DOI: 10.1007/JHEP12(2013)014

[P055-2014] "Revisiting dynamics near a liquid-liquid phase transition in Si and Ga: The fragile-to-strong transition"

Cajahuaringa, S.*; de Koning, M.*; Antonelli, A.*

Using molecular dynamics simulations we analyze the dynamics of two atomic liquids that display a liquid-liquid phase transition (LLPT): Si described by the Stillinger-Weber potential and Ga as modeled by the modified embedded-atom model. In particular, our objective is to investigate the extent to which the presence of a dip in the self-intermediate scattering function is a manifestation of an excess of vibrational states at low frequencies and may be associated with a fragile-to-strong transition (FTST) across the LLPT, as suggested recently. Our results suggest a somewhat different picture. First, in the case of Ga we observe the appearance of an excess of vibrational states at low frequencies, even in the absence of the appearance of a dip in the self-intermediate scattering function across the LLPT. Second, studying the behavior of the shear viscosities traversing the LLPTs we find that both substances are fragile in character above and below their respective LLPT temperatures. Instead of a FTST in an absolute sense these findings are more in line with a view in which the LLPTs are accompanied by a transition from a more fragile to a less fragile liquid. Furthermore, we do not find this transition to correlate with the presence of a dip in the intermediate scattering function.

Journal of Chemical Physics 139[22], 2013. DOI: 10.1063/1.4843415

[P056-2014] "Search for a Higgs boson decaying into a Z and a photon in pp collisions at root s=7 and 8 TeV"

Chatrchyan, S.; Khachatryan, V.; Sirunyan, A. M.; Tumasyan, A.**; Chinellato, J.*; Manganote, E. J. Tonelli***; et al.
CMS Collaboration

A search for a Higgs boson decaying into a Z boson and a photon is described. The analysis is performed using proton--proton collision datasets recorded by the CMS detector at the LHC. Events were collected at center-of-mass energies of 7 TeV and 8 TeV, corresponding to integrated luminosities of 5.0 fb(-1) and 19.6 fb(-1), respectively. The selected events are required to have opposite-sign electron or muon pairs. No excess above standard model predictions has been found in the 120-160 GeV mass range and the first limits on the Higgs boson production cross section times the H -> Z gamma branching fraction at the LHC have been derived.

The observed at 95% confidence level limits are between about 4 and 25 times the standard model cross section times the branching fraction. For a standard model Higgs boson mass of 125 GeV the expected limit at the 95% confidence level is 10 and the observed limit is 9.5. Models predicting the Higgs boson production cross section times the H -> Z gamma branching fraction to be larger than one order of magnitude of the standard model prediction are excluded for most of the 125-157 GeV mass range.

Physics Letters B 726[4-5], 587-609, 2013. DOI: 10.1016/j.physletb.2013.09.057

[P057-2014] "Search for a new bottomonium state decaying to Upsilon(1S)pi(+)pi(-) in pp collisions at root s=8 TeV"

Chatrchyan, S.; Khachatryan, V.; Sirunyan, A. M.; Tumasyan, A.; **Chinellato, J.*; Manganote, E. J. Tonelli*;** et al.
CMS Collaboration

The results of a search for the bottomonium counterpart, denoted as X-b, of the exotic charmonium state X(3872) is presented. The analysis is based on a sample of pp collisions at,root s = 8 TeV collected by the CMS experiment at the LHC, corresponding to an integrated luminosity of 20.7 fb(-1). The search looks for the exclusive decay channel X-b -> Upsilon(1S)pi(+)pi(-) followed by Upsilon(1S) -> mu(+)mu(-). No evidence for an X-b signal is observed. Upper limits are set at the 95% confidence level on the ratio of the inclusive production cross sections times the branching fractions to Upsilon(1S)pi(+)pi(-) of the X-b and the Upsilon(2S). The upper limits on the ratio are in the range 0.9-5.4% for X-b masses between 10 and 11 GeV. These are the first upper limits on the production of a possible X-b at a hadron collider.

Physics Letters B 727[1-3], 57-76, 2013. DOI: 10.1016/j.physletb.2013.10.016

[P058-2014] "Search for Top Squarks in R-Parity-Violating Supersymmetry Using Three or More Leptons and b-Tagged Jets"

Chatrchyan, S.; Khachatryan, V.; Sirunyan, A. M.; Tumasyan, A.; **Chinellato, J.*; Manganote, E. J. Tonelli*;** et al.
CMS Collaboration

A search for anomalous production of events with three or more isolated leptons and bottom-quark jets produced in pp collisions at root s = 8 TeV is presented. The analysis is based on a data sample corresponding to an integrated luminosity of 19: 5 fb(-1) collected by the CMS experiment at the LHC in 2012. No excess above the standard model expectations is observed. The results are interpreted in the context of supersymmetric models with signatures that have low missing transverse energy arising from light top-squark pair production with R-parity-violating decays of the lightest supersymmetric particle. In two models with different R-parity-violating couplings, top squarks are excluded below masses of 1020 GeV and 820 GeV when the lightest supersymmetric particle has a mass of 200 GeV.

Physical Review Letters 111[22], 221801, 2013. DOI: 10.1103/PhysRevLett.111.221801

[P059-2014] "Search for top-squark pair production in the single-lepton final state in pp collisions at"

Chatrchyan, S.; Khachatryan, V.; Sirunyan, A. M.; Tumasyan, A.; **Chinellato, J.*; Tonelli Manganote, E. J.*;** et al.
CMS Collaboration

This paper presents a search for the pair production of top squarks in events with a single isolated electron or muon, jets, large missing transverse momentum, and large transverse mass. The data sample corresponds to an integrated luminosity of 19.5 fb(-1) of pp collisions collected in 2012 by the CMS experiment at the LHC at a center-of-mass energy of . No significant excess in data is observed above the expectation from standard model processes. The results are interpreted in the context of supersymmetric models with pair production of top squarks that decay either to a top quark and a neutralino or to a bottom quark and a chargino. For small mass values of the lightest supersymmetric particle, top-squark mass values up to around 650 GeV are excluded.

European Physical Journal C 73[12], UNSP 2677, 2013. DOI: 10.1140/epjc/s10052

[P060-2014] "Searches for new physics using the t(t)over--bar invariant mass distribution in pp collisions at root s=8 TeV"

Chatrchyan, S.; Khachatryan, V.; Sirunyan, A. M.; Tumasyan, A.; **Chinellato, J.*; Manganote, E. J. Tonelli***; et al.
CMS Collaboration

Searches for anomalous top quark-antiquark production are presented, based on pp collisions at root s = 8 TeV. The data, corresponding to an integrated luminosity of 19.7 fb(-1), were collected with the CMS detector at the LHC. The observed t (t) over bar invariant mass spectrum is found to be compatible with the standard model prediction. Limits on the production cross section times branching fraction probe, for the first time, a region of parameter space for certain models of new physics not yet constrained by precision measurements.

Physical Review Letters 111[21], 211804, 2013. DOI: 10.1103/PhysRevLett.111.211804

[P061-2014] "Signature of bulk longitudinal plasmon-polaritons in the transmission/reflection spectra of one-dimensional metamaterial heterostructures"

Reyes-Gomez, E.; Cavalcanti, S. B.; **Oliveira, L. E.***

A systematic theoretical study of the transmission and reflection spectra of a 1D metamaterial heterostructure consisting of the finite repetition of a double layer of two different building blocks A (normal non-dispersive layer) and B (dispersive metamaterial) is presented, with the multi-layered system sandwiched between two semi-infinite layers of the A material. For the metamaterial slabs B we have studied two different dielectric/magnetic responses: a first one with both the electric permittivity and magnetic permeability given by a Drude-like metamaterial dispersion response, and a second one with the electric permittivity still given by a Drude-like response, whereas the magnetic permeability is given by a more realistic split-ring resonator metamaterial response. Theoretical calculations are performed within the transfer-matrix formalism, and transmission and reflection coefficients of the metamaterial heterostructure are straightforwardly evaluated. For oblique incidence, a finite projection along the growth direction of the electric or magnetic field of the incident wave associated with the TM or TE modes, respectively, leads to a coupling in each layer of the metamaterial heterostructure of the photon modes with the bulk electric or magnetic metamaterial plasmons, respectively. Such photon-plasmon coupling results in the formation of plasmon-polariton modes and gives rise to signatures of the electric or magnetic longitudinal bulk-plasmon polariton modes in the transmission and reflection spectra of the metamaterial heterostructure. Such features survive even in the case of a single AB double-layer metamaterial heterostructure, and experimental observation should be, therefore, easily achieved.

Superlattices And Microstructures 64, 590-600, 2013. DOI: 10.1016/j.spmi.2013.10.029

[P062-2014] "Silicon technology compatible photonic molecules for compact optical signal processing"

Barea, L. A. M.*; Vallini, F.*; Jarschel, P. F.*; Frateschi, N. C.*

Photonic molecules (PMs) based on multiple inner coupled microring resonators allow to surpass the fundamental constraint between the total quality factor (Q(T)), free spectral range (FSR), and resonator size. In this work, we use a PM that presents doublets and triplets resonance splitting, all with high Q(T). We demonstrate the use of the doublet splitting for 34.2 GHz signal extraction by filtering the sidebands of a modulated optical signal. We also demonstrate that very compact optical modulators operating 2.75 times beyond its resonator linewidth limit may be obtained using the PM triplet splitting, with separation of similar to 55 GHz.

Applied Physics Letters 103[20], 201102, 2013. DOI: 10.1063/1.4829743

[P063-2014] "Sol-gel thin-film based mesoporous silica and carbon nanotubes for the determination of dopamine, uric acid and paracetamol in urine"

Canevari, T. C.; Raymundo-Pereira, P. A.; **Landers, R.*; Benvenutti, E. V.*;** Machado, S. A. S.

This work describes the preparation, characterization and application of a hybrid material composed of disordered mesoporous silica (SiO2) modified with multiwalled carbon nanotubes (MWCNTs), obtained by the sol-gel process using HF as the catalyst. This hybrid material was characterized by N-2 adsorption-desorption isotherms, X-ray powder diffraction (XRD), scanning electron microscopy (SEM), high resolution transmission microscopy (HR-TEM), Raman spectroscopy and X-ray photoelectron spectroscopy (XPS). This new hybrid material was used for the construction of a thin film on a glassy carbon electrode. The modified electrode using this material was designated SiO2/MWCNT/GCE. The electrocatalytic properties of the electrode toward dopamine, uric acid and paracetamol oxidation were studied by differential pulse voltammetry. Well-defined and separated oxidation peaks were observed in phosphate buffer solution at pH 7.0, in contrast with the ill-defined peaks observed with unmodified glassy carbon electrodes. The electrode had high sensitivity for the determination of dopamine, uric acid and paracetamol, with the limits of detection obtained using statistical methods, at 0.014, 0.068 and 0.098 mu mol L-1, respectively. The electrode presented some important advantages, including enhanced physical rigidity, surface renewability by polishing and high sensitivity, allowing the simultaneous determination of these three analytes in a human urine sample.

Talanta 116, 726-735, 2013. DOI: 10.1016/j.talanta.2013.07.044

[P064-2014] "Spatial modulation of above-the-gap cathodoluminescence in InP nanowires"

Tizei, L. H. G.*; Zagonel, L. F.*; Tence, M.; Stephan, O.; Kociak, M.; Chiaramonte, T.; **Ugarte, D.*; Cotta, M. A.***

We report the observation of light emission on wurtzite InP nanowires excited by fast electrons. The experiments were performed in a scanning transmission electron microscope using an in-house-built cathodoluminescence detector. Besides the exciton emission, at 850 nm, emission above the band gap from 400 to 800 nm was observed. In particular, this broad emission presented systematic periodic modulations indicating variations in the local excitation probability. The physical origin of the detected emission is not clear. Measurements of the spatial variation of the above-the-gap emission points to the formation of leaky cavity modes of a plasmonic nature along the nanowire length, indicating the wave nature of the excitation. We propose a phenomenological model, which fits closely the observed spatial variations.

Journal Of Physics-Condensed Matter 25[50], 505303, 2013. DOI: 10.1088/0953-8984/25/50/505303

[P065-2014] "Spectral Engineering With CMOS Compatible SOI Photonic Molecules"

Barea, L. A. M.*; Vallini, F.*; de Rezende, G. F. M.*; Frateschi, N. C.*

Photonic systems based on microring resonators have a fundamental constraint given by the strict relationship among free spectral range, total quality factor QT, and resonator size, intrinsically making filter spacing, photonic lifetime, and footprint interdependent. Here, we break this paradigm employing CMOS-compatible silicon-on-insulator photonic molecules based on coupled multiple inner ring resonators. The resonance wavelengths and their respective linewidths are controlled by the hybridization of the quasiorthogonal photonic states. We demonstrate photonic molecules with doublet and triplet resonances with spectral splitting only achievable with single-ring orders of magnitude larger in footprint. In addition, this splitting is potentially controllable based on the coupling (bonds) between resonators. Finally, the spatial distribution of the hybrid states allows up to sevenfold QT enhancement.

IEEE Photonics Journal 5[6], 2202717, 2013. DOI: 10.1109/JPHOT.2013.2289977

[P066-2014] "Synchronisation and stability in river metapopulation networks"

Yeakel, J. D.; Moore, J. W.; Guimaraes, P. R., Jr.; **de Aguiar, M. A. M.***

Spatial structure in landscapes impacts population stability. Two linked components of stability have large consequences for persistence: first, statistical stability as the lack of temporal fluctuations; second, synchronisation as an aspect of dynamic stability, which erodes metapopulation rescue effects. Here, we determine the influence of river network structure on the stability of riverine metapopulations. We introduce an approach that converts river networks to metapopulation networks, and analytically show how fluctuation magnitude is influenced by interaction structure. We show that river metapopulation complexity (in terms of branching prevalence) has nonlinear dampening effects on population fluctuations, and can also buffer against synchronisation. We conclude by showing that river transects generally increase synchronisation, while the spatial scale of interaction has nonlinear effects on synchronised dynamics. Our results indicate that this dual stability - conferred by fluctuation and synchronisation dampening - emerges from interaction structure in rivers, and this may strongly influence the persistence of river metapopulations.

Ecology Letters 17[3], 273-283, 2014. DOI: 10.1111/ele.12228

[P067-2014] "Synchrotron X-ray diffraction and Raman spectroscopy of Ln(3)NbO(7) (Ln=La, Pr, Nd, Sm-Lu) ceramics obtained by molten-salt synthesis"

Siqueira, K. P. F.; Soares, J. C.; **Granado, E.*;** Bittar, E. M.; de Paula, A. M.; Moreira, R. L.; Dias, A.

Ln(3)NbO(7) (Ln=La, Pr, Nd, Sm, Eu, Gd, Tb, Dy, Ho, Er, Tm, Yb, and Lu) ceramics were obtained by molten-salt synthesis and their structures were systematically investigated by synchrotron X-ray diffraction (SXRD), second harmonic generation (SHG) and Raman spectroscopy. It was observed that ceramics with the largest ionic radii (La, Pr, Nd) crystallized into the Pmcn space group, while the ceramics with intermediate ionic radii (Sm-Gd) exhibited a different crystal structure belonging to the Ccmm space group. For this last group of ceramics, this result was corroborated by SHG and Raman scattering and ruled out any possibility for the non-centrosymmetric C222(1) space group, solving a recent controversy in the literature. Finally, according to SXRD, Tb-Lu containing samples exhibited an average defect fluorite structure (Fm (3) over barm space group). Nonetheless, broad scattering at forbidden Bragg reflections indicates the presence of short-range domains with lower symmetry. Vibrational spectroscopy showed the presence of six Raman-active modes, inconsistent with the average cubic fluorite structure, and in line with the existence of lower-symmetry nano-domains immersed in the average fluorite structure of these ceramics.

Journal Of Solid State Chemistry 209, 63-68, 2014. DOI: 10.1016/j.jssc.2013.10.015

[P068-2014] "Tailoring Thermal Transport Property of Graphene through Oxygen Functionalization"

Hengji Zhang, **Alexandre F. Fonseca*,** Kyeongjae Cho

We compute thermal conductivity of graphene oxide at room temperature with molecular dynamics simulation. To validate our simulation model, we have investigated phonon scattering in graphene due to crystal boundary length and isotope defect, both of which are able to diagnose the behavior of long wavelength and short wavelength phonon scattering. Our simulation shows that thermal conductivity of pristine graphene has logarithmic divergence for the boundary length up to 2 μm. As compared with pristine graphene, thermal conductivity of graphene oxide can be reduced by a factor of 25 at low oxygen defect concentration. Moreover, we find that not only the concentration but also the configuration of the oxygen functional groups (e.g., hydroxyl, epoxide, and ether) has significant influence on the thermal conductivity. Through phonon mode analysis, phonon defect scattering as well as phonon localization are mainly responsible for the conspicuous reduced thermal conductivity. The simulation results have provided fundamental insight on how to precisely control thermal property of graphene oxide for thermal management and thermoelectric applications.

The Journal of Physical Chemistry C 118[3], 1436-1442, 2014. DOI: 10.1021/jp4096369

[P069-2014] "The asymmetric Goos-Hanchen effect"

Araujo, M. P.*; Carvalho, S. A.; De Leo, S.

We show under which conditions optical Gaussian beams, propagating throughout an homogeneous dielectric right angle prism, present an asymmetric Goos-Hanchen (GH) effect. This asymmetric behavior is seen for incidence at critical angles and happens in the propagation direction of the outgoing beam. The asymmetric GH effect can also be seen as an amplification of the standard GH shift. Due to the fact that it only depends on the ratio between the wavelength and the minimal waist size of the incoming Gaussian beam, it can also be used to determine one of these parameters. Multiple-peak interference is an additional phenomenon seen in the presence of such asymmetric effects.

Journal Of Optics 16[1], 015702, 2014. DOI: 10.1088/2040-8978/16/1/015702

[P070-2014] "The effect of noble gas bombarding on nitrogen diffusion in steel"

Ochoa, E. A.*; Droppa, R.; Basso, R. L. O.; **Morales, M.*; Cucatti, S.*; Zagonel, L. F.*;** Czerwiec, T.; dos Santos, M. C.; Figueroa, C. A.; Alvarez, F.

The low energy (similar to 50-350 eV) noble gases ion bombardment of the steel surface shows that the pre-treatments increase nitrogen diffusion by modifying the outermost structure of the material. The surface microstructure and morphology of the studied samples were characterized by Scanning Electron Microscopy (SEM) and Atomic Force Microscopy (AFM). The crystalline and chemical structures in the outermost layers of the surface were analyzed by grazing angle X-ray diffraction (GAXRD) and photoemission electron spectroscopy (XPS). Temperature effusion studies of the implanted ions are used to elucidate the noble gases site localization in the network. The local compressive stress induced by the nearby iron atoms on the core level electron wave functions of the trapped noble gases are studied by photoemission electron spectroscopy (XPS) and interpreted considering a simple mechanical model. Nano-hardness measurements show the dependence of the material elastic constant on the energy of the implanted noble gases. Although the ion implantation range is about few nanometers, the atomic attrition effect is larger enough to modify the material structure in the range of micrometers. Two material stress zones were detected where the outermost layers shows compressive stress and the underneath layers shows tensile stress. The implanted noble gases can be easily removed by heating. A diffusion model for polycrystalline-phase systems is used in order to discuss the influence of the atomic attrition on the N diffusion coefficient. The concomitant effect of grain refining, stress, and surface texture on the enhancing nitrogen diffusion effect is discussed.

Materials Chemistry And Physics 143[1], 116-123, 2013. DOI: 10.1016/j.matchemphys.2013.08.027

[P071-2014] "The electron-phonon interaction from fundamental local gauge symmetries in solids"

Dartora, C. A.; **Cabrera, G. G.***

The elastic properties of solids are described in close analogy with General Relativity, by locally gauging the translational group of space-time. Electron interactions with the crystal lattice are thus generated by enforcing full gauge invariance, with the introduction of a gauge field. Elementary excitations are associated with the local gauge, contrasting to the usual interpretation as Goldstone bosons emerging from global symmetry breaking. In the linear limit of the theory, the gauge field displays elastic waves, that we identify with acoustic phonons, when the field is quantized. Coupling with the electronic part of the system yields the standard electron-phonon interaction. If spin-orbit effects are included, unusual couplings emerge between the strain field and the electronic spin current, leading to novel physics that may be relevant for spintronic applications.

Journal Of Physics A-Mathematical And Theoretical 47[3], 035004, 2014. DOI: 10.1088/1751-8113/47/3/035004

[P072-2014] "Tuning the surface anisotropy in Fe-doped NiO nanoparticles"

Moura, K. O.*; Lima, R. J. S.; **Coelho, A. A.***; Souza-Junior, E. A.; Duque, J. G. S.; Meneses, C. T.

Ni1-xFexO nanoparticles have been obtained by the co-precipitation chemical route. X-ray diffraction analyses using Rietveld refinement have shown a slight decrease in the microstrain and mean particle size as a function of the Fe content.

The zero-field-cooling (ZFC) and field-cooling (FC) magnetization curves show superparamagnetic behavior at high temperatures and a low temperature peak (at T = 11 K), which is enhanced with increasing Fe concentration. Unusual behavior of the coercive field in the low temperature region and an exchange bias behavior were also observed. A decrease in the Fe concentration induces an increase in the exchange bias field. We argue that these behaviors can be linked with the strengthening of surface anisotropy caused by the incorporation of Fe ions.

Nanoscale 6[1], 352-357, 2014. DOI: 10.1039/c3nr04926d

Proceedings

[P073-2014] "Engineered dynein light chain Rp3: a strategy to exploit cell's machinery for an enhanced intracellular trafficking of transgenes"

Favaro, M. T. P.; de Toledo, M. A. S.; Alves, R. F.; **Janissen, R.*;** Souza, A. P.; Azzoni, A. R.

Human Gene Therapy 24[12], A63-A63, 2013.

Collaborative Congress of the European-Society-for-Gene-and--Cell-Therapy and the Spanish-Society-for-Gene-and-Cell-Therapy, Madrid, SPAIN, 25-28j Out 2013.

[P074-2014] "Strange and Multi-Strange Particle Production in ALICE"

Chinellato, D. D.*
IOP
ALICE Collaboration

The production of strange and multi-strange hadrons in proton-proton (pp) and lead-lead (Pb-Pb) collisions is studied with the ALICE experiment at the CERN LHC. These particles are reconstructed via their weak decay topologies, exploiting the tracking and particle identification capabilities of ALICE. Measurements of central rapidity yields of Lambda, Xi(-) and Omega(-) baryons, their antiparticles and K-S(0) mesons are presented as a function of transverse momentum for Pb-Pb collisions at \/s(NN) = 2.76 TeV. They are compared to those observed in pp collisions as well as to results from lower energy nucleus-nucleus measurements.

HOT QUARKS 2012: WORKSHOP FOR YOUNG SCIENTISTS ON THE PHYSICS OF ULTRARELATIVISTIC NUCLEUS-NUCLEUS COLLISIONS. Série: Journal of Physics Conference Series 446, UNSP 012055, 2013. DOI: 10.1088/1742-6596/446/1/012055

Workshop for Young Scientists on the Physics of Ultrarelativistic Nucleus-Nucleus Collisions (Hot Quarks), 5th, PR, 14-20 Out 2012.

Correções

[P075-2014] "A study on analytic parametrizations for proton-proton cross-sections and asymptotia (vol 40, 125001, 2013)"

Menon, M. J.*; Silva, P. V. R. G.*

Journal Of Physics G-Nuclear And Particle Physics 41[1], 019501, 2014. DOI: 10.1088/0954-3899/41/1/019501

***Autores da comunidade IFGW.**

Defesas de Teses - Mestrado

[D001-2014] "Contribuições de trajetórias complexas ao propagador semiclássico para estados coerentes"
Aluno: Wendell Pereira Barreto
Orientador: Prof. Dr. Marcus A. M. de Aguiar
Data: 07/01/2014

[D002-2014] "Violação de CP em oscilações de neutrinos"
Aluno: Rafael Noberto Almeida da Costa
Orientador: Prof. Dr. Marcelo Moraes Guzzo
Data: 14/02/2014

Defesas de Teses - Doutorado

[T001-2014] "Nanoscrolis e outras nanoestruturas"
Aluno: Eric Perim Martins
Orientador: Prof. Dr. Douglas Soares Galvão
Data: 25/02/2014

[T002-2014] "Simulações de sistemas em nanoescala: Membranas de grafeno e espectroscopia fora do equilíbrio"
Aluno: Gustavo Brunetto
Orientador: Prof. Dr. Douglas Soares Galvão
Data: 25/02/2014

[T003-2014] "Estudo de filmes ultra finos de óxidos 'high-K' crescidos sobre semicondutores"
Aluno: Marcelo Falsarella Carazzolle
Orientador: Prof. Dr. Richard Landers
Data: 27/02/2014

Fonte: Portal IFGW/PPós-graduação.
Disponível em: http://portal.ifi.unicamp.br/eventos#date=2013-05-01,mode=month

*A partir de 2014 o Boletim Abstracta será somente em versão eletrônica. Acesse o portal Abstracta e faça seu cadastro como leitor, para receber em seu email a notificação de cada novo número publicado:

<http://abstracta.ifi.unicamp.br>

Abstracta

Instituto de Física
Diretor: Prof. Dr. Daniel Pereira
Diretor Associado: Prof. Dr. Newton Cesario Frateschi
Universidade Estadual de Campinas - UNICAMP
Cidade Universitária Zeferino Vaz
13083-859 - Campinas - SP - Brasil
e-mail: secdir@ifi.unicamp.br
Fone: 0XX 19 3521-5300

Publicação

Biblioteca do Instituto de Física Gleb Wataghin
http://portal.ifi.unicamp.br/biblioteca

Diretora Técnica: Sandra Maria Carlos Cartaxo
Coordenador da Comissão de Biblioteca: Prof. Dr. André Koch Torres de Assis

Elaboração
Maria Graciele Trevisan (Bibliotecária)
graciele@ifi.unicamp.br

Projeto Gráfico
ÍgneaDesign

Impressão: Gráfica Central - Unicamp